Small-Angle Neutron Scattering Studies of Inhomogeneities in Latex Particles from Emulsion Homopolymerizations

Martin F. Mills,† Robert G. Gilbert,* and Donald H. Napper

School of Chemistry, Sydney University, Sydney, NSW 2006, Australia

Adrian R. Rennie and Ronald H. Ottewill

Department of Chemistry, University of Bristol, Bristol BS8 1TS, U.K.

Received December 4, 1992; Revised Manuscript Received February 26, 1993

ABSTRACT: Small-angle neutron scattering experiments were carried out to examine the extent of monomer/polymer spatial inhomogeneities in latex particles formed in an emulsion homopolymerization, using contrast variation and isotopic labeling systems to look at the morphology of swollen and two-stage latices. Samples covered a range of molecular weights including systems where the radius of gyration of the polymer chains was both comparable to and smaller than the particle size. The experiments were designed to test separately inhomogeneities arising from two different effects: (1) the "repulsive wall" (thermodynamic) effect arising from the decrease in entropy of a polymer chain confined near the surface of a particle (the experiments here examined polymer distribution in polystyrene particles swollen with toluene); (2) "surface anchoring" (largely kinetic) arising mainly because, with a water-soluble initiator, free radicals enter latex particles at the surface (here experiments examined the distribution of newly formed polymer in seeded growth; related to this are inhomogeneities arising from finite rates of diffusion of monomer and of polymer). Results support the conclusion that repulsive wall effects do not give rise to significant nonuniformities but that inhomogeneities may arise in the final product where the polymer chain dimensions are substantially less than the particle radius. The latter conclusion is consistent with predictions of the surface anchoring model.

Introduction

The question of the extent of spatial inhomogeneity that will be found in the distribution of polymer in a latex particle formed by the emulsion polymerization of a single monomer is important from several points of view. First, most mechanistic interpretations and predictions of the kinetics of latex particle formation and growth presume homogeneity, and if significant inhomogeneities were to be found under conventional conditions, much of this body of knowledge would be of questionable validity. Second, the design and control of particle morphology is of considerable technical importance in latex copolymers used in, for example, surface coatings; morphology control is by both thermodynamic (e.g., polymer incompatibility) and kinetic (e.g., starved feed) means, and improved knowledge of the underlying chemical physics leading to inhomogeneity will clearly be obtained from a study of this behavior in systems comprising a single monomer and its polymer.

The origins of inhomogeneity in a latex particle formed from a single monomer fall into two basic classes. The first comprises kinetic effects arising because entry (when using a water-soluble initiator) and exit of free radicals into latex particles occurs perforce at the particle surface: e.g., the effect known as *surface anchoring*, whereby the charged end group of the entering free radical remains attached to the surface; this class includes any effects arising from diffusion becoming rate-determining within the particle. The second class comprises thermodynamic, or repulsive wall, effects, which for a single monomer/polymer system arise from the entropic tendency of a polymer chain to stay away from the confined region of a particle surface. There has been considerable effort expended on the problem of latex particle inhomogeneity from a theoretical viewpoint, reviewed elsewhere.[1,2] From this work has emerged a better understanding of the role of surface anchoring and repulsive wall effects in determining particle morphology, enabling predictions to be made as to the conditions under which either of these mechanisms is likely to lead to significant nonuniformity. As discussed further below, there have also been a number of experimental investigations of inhomogeneities, usually using two-stage growth, wherein the second-stage polymerization is on a preformed seed. Unfortunately, the conclusions which may be drawn from these results are limited, primarily because of the following considerations.

(1) The nature of the system is not conducive to experimental investigation, because of the small length scale of inhomogeneities and because the second-stage polymer is physically indistinguishable from that of the seed. The first of these problems limits the experimental techniques which may be used because of the high resolution required while the second means that some form of label must be used to differentiate between stage 1 and stage 2 polymers—more often than not, this label may perturb the kinetics and thermodynamics of the system, rendering the results open to question. Even where these problems are overcome, it is difficult to obtain results of sufficient quality to characterize the morphology fully.

(2) Partly due to inadequate theoretical development, experiments have not in general been designed to test specific mechanisms. For example, molecular weight data are not usually available, primarily because its significance has not generally been appreciated. Indeed, in the only case hitherto when such data have been presented,[3,4] there were some uncertainties associated with the experimental method: the data were obtained only at a single contrast, the use of a blank subtraction to obtain information at low Q in a multicomponent, multiphase system (the results are sensitive to this because of the possibility of different polydispersities in the blank and sample), and the data at very low Q could have significant contributions from interparticle interactions. Furthermore, fairly diverse polymerization conditions tend to be used which may be inadequately documented, rendering it difficult to estimate

* Author to whom correspondence is addressed.
† Present address: Technical Centre, Du Pont (Australia), Lot 15, Newton Rd., Wetherill Park, NSW 2164, Australia.

0024-9297/93/2226-3553$04.00/0

the relevant rate parameters and concentrations.

The present work uses small-angle neutron scattering (SANS) from isotropically labeled systems to study the morphology of latex particles both at an intermediate stage of polymerization and after its completion. This technique has the advantage that deuteration leads to minimal perturbation of the system.

Previous Experimental Investigations of Inhomogeneities

Some experimental support for the surface anchoring models has been put forward by Chen and Lee,[5] who based their technique on the pioneering work of Grancio *et al.*[6] in which trace amounts of butadiene/isoprene were used as a label in a seeded styrene emulsion system. The particles were subsequently sectioned, stained, and examined by electron microscopy, results clearly showing that, for large particles most of the butadiene/isoprene introduced was polymerized in a shell around the outside of the particles. It was found however that smaller particles or systems in which oil-soluble initiator was used showed no evidence of inhomogeneity, these observations being consistent with predictions of the surface anchoring model. One difficulty with the technique is that small differences in the polymer composition may cause incompatibility effects and consequent phase separation of the two polymers. This is compounded by the possibility that butadiene may cause cross-linking of the second polymer formed, producing a polymer network having very different characteristics to the styrene homopolymer of the first stage. While polymer films produced by casting the dissolved latex onto a flat surface show no obvious heterogeneities, this possibility cannot be dismissed. The conclusions of Chen and Lee were contrary to those of Grancio and Williams,[6] who were the first to put forward theoretical and experimental evidence for the repulsive wall effect. Their experiments on the morphology of a two-stage styrene emulsion polymerization with a butadiene label showed that most of the butadiene was located near the surface after the completion of polymerization, this observation being over a wide range of particle sizes and in systems where oil-soluble initiator was used, albeit to a lesser extent.[7] However, it has been shown that most growth in emulsion polymerizations with an oil-soluble initiator comes from free radicals generated from the small amount of initiator present in the aqueous phase.[8,9] Further experiments, in which tritium labeling of the seed was used, were interpreted as follows: in nonuniform particles in which the (nonlabeled) shell was sufficiently thick, emitted β-particles were unable to escape from the latex, while homogeneous particles allowed escape of β-emission.[10] However, since the path length of a β-particle in organic media is *ca.* 1 μm and the particles used were somewhat smaller than this, the results are somewhat inconclusive. Chang and Chen[11] also carried out kinetic studies in large (500-nm) diameter particles with relatively low molecular weight (10^4–10^6) chains, which appeared to support the presence of inhomogeneities therein. This was attributed to surface anchoring effects, although we note parenthetically that a comparative study with much smaller particles would have been particularly useful in the context of testing inferences from kinetic effects.

Data providing information on the nature of surface anchoring were provided by conductometric titrations of the exposed sulfate end groups in polystyrene latexes.[12] Results suggested that a large proportion of the sulfate groups remained on the particle surface (as one might expect), although in some instances there were also significant amounts of sulfate in the particle interior. This raises the question of whether some of the old polymer end groups are swallowed into the particle as new polymer is formed near the surface. While it is evident that there would be a considerable enthalpic barrier to this, it is also clear that not all of the polymer present can maintain its unperturbed conformation near the particle surface. At low conversions, polymer formed in the first and second stages may not be distinguished because of interdiffusion of polymer chains (beyond the glass transition). The morphology (i.e., distribution of polymer) may then be more a function of the relative molecular weights (and hence penetration) of the seed and the second stage. At high conversions, when the system is glassy (above *ca.* 85% polymer for styrene at 50 °C), polymer chains will be effectively frozen in place; this is the origin of morphology predicted in earlier simulations.[1]

Linne *et al.*[13] carried out SANS experiments on isotopically labeled latexes in which the first and second stages were respectively protonated and deuterated polystyrene. Contrast matching and blank subtraction were used as described below to remove unwanted contributions from the scattering, leaving in principle only scattering due to individual polymer chains, together with any morphology or "collective" chain structure which may be present. The "blank" here consisted of a latex prepared under the same conditions as the sample but in which the polymer was a statistical copolymer of the protonated and deuterated monomers. It was found that for certain samples an anomalously high molecular weight was obtained for the polymer chains, this being taken to be a measure of chain aggregation: in effect, particle inhomogeneity. It was concluded that maximum inhomogeneity is obtained when the ratio of the polymer radius of gyration to the particle radius is approximately 0.2. This was explained as follows: when the chain dimensions are very much less than the particle radius, the thickness of the depletion layer is correspondingly small. Conversely, if the chain dimensions are comparable to the size of the particle, the polymer chains will be highly compressed and will exert a force outward, countering the repulsive effect of the surface. Data were also obtained for swollen latexes in which the added monomer was deuterated, results showing similar behavior to the fully polymerized systems. This seemed to support the conclusion that the morphology was a consequence of repulsive wall rather than surface anchoring effects. A more recent publication[14] suggested agreement between that model and experiment; however, this random flight model does not consider excluded volume, which as discussed elsewhere[2] neglects some important effects (e.g, it predicts that the density approaches zero at the particle surface). An alternative explanation of these data is possible, and for this reason the present study using contrast variation was performed. Our approach is to fit the observed scattering from appropriately labeled latex particles to the form factors of either a core–shell or a homogeneous sphere model for the particle form factor as appropriate. Similar methods have been applied by Fisher *et al.*[15] to examine the morphology of labeled poly(methyl methacrylate) homo- and copolymer systems (the data being found to fit a core–shell model). Results were also obtained by this method by Harris *et al.*[16] for swollen polystyrene latexes, the data being found to be consistent with homogeneous mixing of polymer and monomer. Unfortunately, molecular weight data are not available for these experiments, so it is not possible to test fully the validity of either mechanism with these results.

Table I. Latex Characteristics[a]

Seed Latexes

seed	monomer	R (nm)	σ (nm)	M_W	M_N	R_g (nm)	R_g/R
LS4	styrene	67	4	6.5×10^5	2.9×10^5	22	0.3
S40NM	styrene	44	4	1.8×10^6	7.2×10^5	37	0.8
DEU10	styrene-d_8	56	4	2.4×10^6	9.7×10^5	43	0.8

Seeded Polymerizations

sample	seed	R (nm)	σ (nm)	M_W[b]	M_N[b]	R_g (nm)	R_g/R
DEU3	S40NM	55	6	$>2 \times 10^6$			
DEU7	S40NM	58	5	1.1×10^6	3.7×10^5	29	0.5
DEU11	LS4	80	4	8.8×10^5	2.7×10^5	26	0.3

[a] R = latex radius; σ = standard deviation; R_g = radius of gyration of polymer chains computed from M_W). [b] These values are for the second-stage polymer only.

Testing the Models

In the present studies, contrast variation techniques[17] are used, in which different features of the particle morphology are highlighted as the relative coherent scattering densities (analogous to changes in refractive index in a light scattering experiment) of the particle and the surrounding medium are changed. This variation is achieved by changing the isotopic composition of the samples and relies upon the large difference in the scattering cross section of H and D atoms. It is found that this provides a less ambiguous view of the particle structure than the result at a single contrast which may not be unique to the morphology under consideration. Specifically, the form of the scattering from a homogeneous sphere is essentially independent of contrast, simply scaling in intensity as the contrast is changed. When there is no contrast between the particle and the continuous phase, there will be essentially no structure visible and there will be zero scattering (except for background). On the other hand, the scattering function (form factor) for a particle having internal structure will show changes in behavior as the contrast is varied. These changes in the scattering are used in model fitting in order to obtain information about the particle morphology. Contrast between the particles and the aqueous phase and between the constituents within the particles themselves was achieved by using deuterium as an isotopic label. This provides a ready means of distinguishing between species while minimally perturbing the chemistry of the system. Scattering for each sample was measured over a range of contrasts by varying the H_2O/D_2O ratio in the aqueous phase. As will be seen, the scattering from latex particles having internal structure is found to be particularly sensitive to variations in contrast of the aqueous medium so that any morphology which might be overlooked or difficult to interpret in the scattering at a single contrast should be better characterized in this manner.

The work of this paper has the specific aim of discerning from the experimentally determined morphologies which (if either) of the proposed mechanisms for nonuniform polymerization is operative in typical styrene emulsion polymerizations; the tests also serve as a general indication of the repulsive wall effect for any polymer. It is of course possible at the outset that both mechanisms are important and that the morphology is the product of interplay between the two.

Method for Testing the Repulsive Wall Model. Repulsive wall effects were investigated by looking for evidence of nonuniformity in latexes swollen with toluene. Toluene was used in place of monomer (in this case styrene) because of the reactivity of the latter. Two seed latexes were prepared having the characteristics predicted by Linne and co-workers[13] to show maximum inhomogeneity from repulsive wall effects: i.e., the ratio of the polymer radius of gyration to the particle radius should be in the range 0.1–0.5. The first of these seeds was composed of polystyrene and the second of poly(perdeuterostyrene). The seeds were swollen on an equal weight-for-weight basis with perdeuterotoluene and toluene respectively, and the scattering was measured at several contrasts. The resulting scattering curves were fitted to homogeneous sphere or core–shell models as appropriate.

Method for Testing the Surface Anchoring Model. To examine the effect of surface anchoring, seeded polymerizations were carried out in which the seed and second-stage polymers were distinguished by isotopic labeling. The morphology of the resulting two-stage latex was then investigated by SANS. Interpretation of the results is contingent on the conclusions given above: if swelling is found to be uniform but first- and second-stage polymers are not uniformly mixed, it must presumably be due to surface anchoring rather than repulsive wall effects.

In these experiments, the seed polymer used was polystyrene and the second-stage polymer was poly(perdeuterostyrene). Polymerization conditions were varied with the aim of giving second-stage polymer of low and high molecular weight in seeds of varying radius. The molecular weight distribution in emulsion systems of this type is generally transfer dominated at 50 °C[18] and so increasing the initiator concentration will not necessarily alter the molecular weight. It may however alter the fraction of *anchored* chains in the system.[1]

Characteristics of all latexes used are given in Table I. Only a limited range of samples is represented, due in part to experimental difficulties. Molecular weights were generally slightly lower than expected, possibly because of a trace impurity which may have been acting as a chain-transfer or stopping agent. However, this is not thought to affect the validity of any conclusions regarding surface anchoring effects as discussed later.[1] The same procedures as for the seed and swollen latexes were used for measurement of scattering from these samples.

Experimental Section

Materials. The source and chemical purity of all chemicals used is as follows: styrene (Ajax Chemicals, A.R. grade); styrene-d_8 (Sigma, 98+ atom % D, 0.5% hydroquinone as inhibitor); $NaHCO_3$ (Merck, A.R. grade); $K_2S_2O_8$ (Merck, A.R. grade); Aerosol MA80 (AMA, sodium dihexylsulfosuccinate, Cyanamide Australia, industrial grade); sodium dodecyl sulfate (Pierce Chemicals, 99% purity); $Na_2S_2O_5$ (Merck, A.R. grade); D(−)-Fructose (Ajax Chemicals, A.R. Grade); H_2O (double distilled from alkaline permanganate); D_2O (distilled, 98+ atom % D); NaCl (Merck, A.R. Grade). Styrene was distilled under vacuum to remove inhibitors. Inhibitors were removed from perdeuterostyrene by washing three times with a 5 mol dm^{-3} NaOH

Table II. Recipes (All Weights in Grams)

	seed		
	DEU10	LS4	S40NM
styrene		131.06	3.92
styrene-d_8	1.0		
AMA	0.043	5.6	0.17
$NaHCO_3$	0.0034	0.44	0.0158
$K_2S_2O_8$	0.0036	0.44	0.157
H_2O	2.85	373.45	9.79
temp (°C)	80	90	80
% solids	25.8	25.6	28.2

	seeded polymerization		
	DEU3	DEU7	DEU11
seed latex	S40NM	S40NM	LS4
seed weight	4.01	2.01	2.06
styrene-d_8	1.23	0.65	0.54
SDS	0.0080	0.010	0.010
$NaHCO_3$	0.0020	0.016	0.013
$K_2S_2O_8$	0.0020	0.016	0.022
H_2O	5.00	18.80	18.20
$FeCl_3$			0.0010
$Na_2S_2O_5$			0.013
fructose			0.17
% solids	23	6.0	5.6
temp (°C)	50	50	50

solution and a further times with doubly distilled water. All other chemicals were used as received.

Seed Latexes. Seed latexes were prepared in a bottle polymerizer at elevated temperature, seed recipes and polymerization temperatures being given in Table II. Predissolved initiator was added to the reaction mixture and the emulsion purged with nitrogen immediately prior to polymerization. Seed latex LS4 was dialyzed after completion of polymerization in order to remove surfactant.

Swollen Latexes. Swelling was achieved by adding surfactant and toluene to the latex (protonated to deuterated, and *vice versa*) and stirring overnight. Results of earlier scattering studies[16] indicate that swelling is complete within several hours. Seed latexes were diluted to 1.25% by weight polymer, while in the case of swollen and two-stage latexes, total organics constituted 2.5% of the total weight. For all samples 1×10^{-3} mol dm^{-3} NaCl was added to the aqueous phase in order to minimize electrostatic interparticle interactions.

Seeded Polymerizations. Monomer and surfactant were added to the seed latex, which was then allowed to swell by shaking at room temperature overnight. Initiator and buffer were then added and the samples polymerized at elevated temperature. Quantities and temperatures are given in Table II. Redox agents ($FeCl_3$, $Na_2S_2O_5$, fructose) were added to DEU11 in an attempt to increase the termination rate by accelerating free-radical production.

Latex Characterization. Particles were photographed at a magnification of 10 000× using transmission electron microscopy and counted using a Carl–Zeiss particle size analyzer with an internal standard.[19] Results are in good agreement with data obtained from photon correlation spectroscopy when proper account is taken of double-layer effects and conversion from Z-average to number average. Molecular weight distributions were measured by gel permeation chromatography with a Polymer Laboratories 30-cm Ultrastyragel mixed-bed column using Polymer Laboratory polystyrene standards. In the case of seeded polymerization where molecular weight distributions of the first- and second-stage polymerizations were overlapping, the second-stage molecular weight distribution was obtained by subtracting the previously measured contribution due to the seed.[20,21] The radius of gyration may be estimated from the molecular weight if it is assumed that the polymer chain forms a Gaussian coil. For polystyrene, the following relationship may then be used:[22]

$$R_g = 0.275(M_W)^{1/2} \quad (1)$$

where M_W is the weight-average molecular weight in atomic mass units and R_g is in angstroms. Due to uncertainties in subtraction of the seed contribution for sample DEU3 (see Table I), accurate molecular weight distributions could not be obtained; nevertheless, it can be stated that the second-stage growth in this seed is of significantly higher M_W than that in the other two samples.

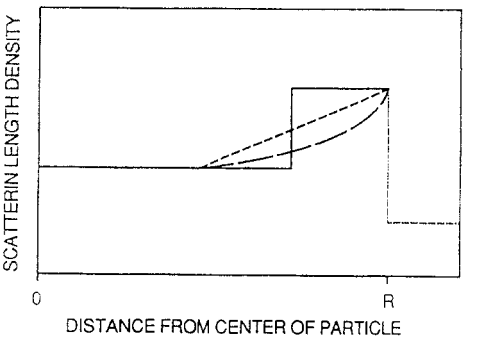

Figure 1. Examples of profiles used to describe particle morphology. (– –) Profile predicted by surface anchoring model. (—) Core–shell model. (- - -) Ramp function.

Small-Angle Neutron Scattering

The total scattering amplitude from a group of nuclei is given by the sum of the individual amplitudes from each of the nuclei. This expression is readily evaluated for a *single* homogeneous or core–shell particle (as illustrated schematically in Figure 1) to give the following analytic form:[23,24]

$$I(Q) = \frac{16\pi^2}{9}\Bigg[(\rho_s - \rho_m)3R_s^3\left(\frac{\sin(QR_s) - QR_s\cos(QR_s)}{(QR_s)^3}\right) - (\rho_s - \rho_m)3R_c^3\left(\frac{\sin(QR_c) - QR_c\cos(QR_c)}{(QR_c)^3}\right) + (\rho_c - \rho_m)3R_c^3\left(\frac{\sin(QR_c) - QR_c\cos(QR_c)}{(QR_c)^3}\right)\Bigg]^2 \quad (2)$$

where R_c and R_s are the radii of the core and shell, ρ_c and ρ_s are the corresponding coherent scattering length densities, and ρ_m is the coherent scattering length density of the surrounding medium. In this equation, the scattering vector Q for elastic scattering is given by:

$$Q = \frac{4\pi}{\lambda}\sin\frac{\theta}{2} \quad (3)$$

where λ is the wavelength of the incident radiation and θ the scattering angle. This expression simplifies in the special case of a homogeneous sphere because of cancellation of the second and third terms in the equation. The scattering function of eq 2 shows characteristic maxima and minima, the positions of these extrema being a function of the particle size. For nonhomogeneous particles, the positions of the minima will also be a function of the contrast.

The reasons for this may be understood when it is noted that, if the scattering length density of the medium is matched to that of the shell, the illusion of scattering being from a smaller particle is presented, while if the medium is matched to the core, a hollow sphere structure is observed. The change in behavior (see, e.g., Figure 2) resulting from such variation in contrast is found to be a particularly useful indicator of the morphology,[17] giving a far more stringent test of the model used than measurement of the scattering at only one contrast.

Scattering experiments were performed using the neutron diffractometer D11 at the Institut Laue-Langevin at Grenoble, France. A wavelength of 0.8 nm was used at three sample detector distances (5, 20, and 37.5 m) in order to cover a range of scattering vectors from 0.02 to 0.6 nm^{-1}. The data obtained using a two-dimensional detector were

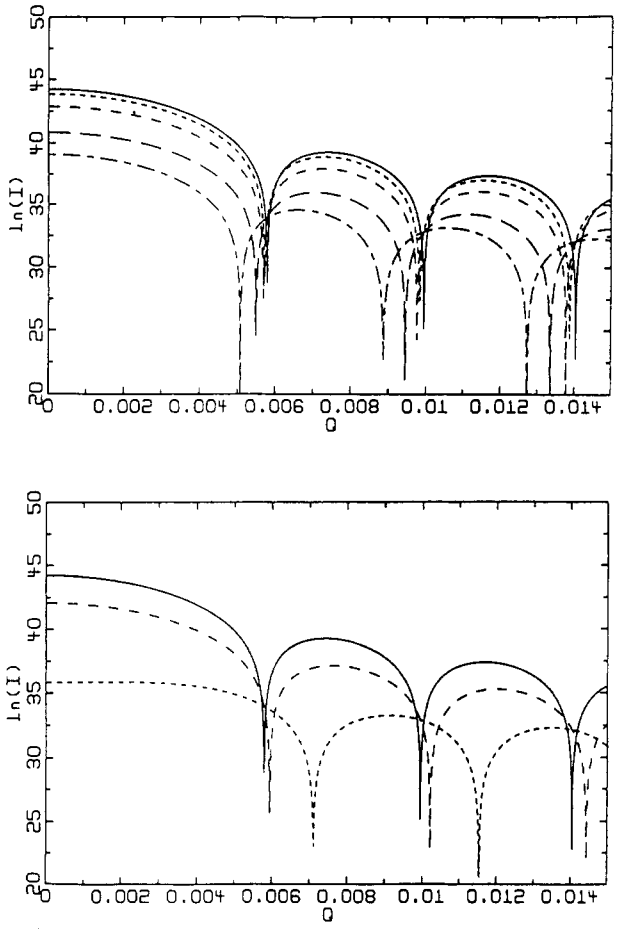

Figure 2. Effect of contrast variation on the scattering function for a core–shell particle. Parameters as for two-stage latex DEU11. Top: (···) 20% D_2O; (- - -) 40% D_2O; (– –) 60% D_2O; (– · –) 65% D_2O; (—) equivalent homogeneous particle. Bottom: (···) 70% D_2O; (- - -) 90% D_2O; (—) equivalent homogeneous particle.

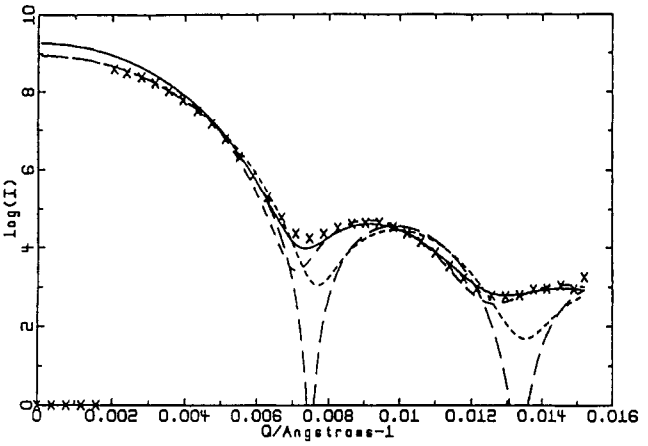

Figure 3. Effect of instrument resolution and polydispersity on fitted curves (sample DEU7, 20% D_2O, parameters as in Table IV). In this and subsequent figures, points where log $I = 0$ are there to show the extent of the beam stop. (×) Experiment. (—) No polydispersity or resolution function. (···) Instrument resolution only. (- - -) Polydispersity only. (– –) Polydispersity and instrument resolution.

radially averaged and then corrected for background scattering using blank spectra from the dispersion medium, e.g., an H_2O/D_2O mixture having the same composition as that used to prepare the sample: this is a standard procedure.[25] Conversion of the scattering intensities into absolute values was carried out using the results obtained from water as a reference material. The method generally used for this normalization has been presented in detail elsewhere.[16,25-27]

Only at the largest values of Q is the incoherent background scattering from water significant. In this region, careful subtraction of the dispersion medium is required. However, it is convenient to normalize to the water standard in this region, i.e., a sample detector distance of 5 m. When using an equivalent D_2O/H_2O mixture as background for the sample, a small error is introduced because of the volume occupied by solids in the sample. This was corrected using the known composition of the samples but was found not generally to have a significant impact on the results obtained.

Analysis of the data was carried out by fitting theoretically computed curves to the experimental data in the intermediate Q range.[28]

The scattering function was calculated using the particle form factor for scattering from concentric spheres combined with a log-normal distribution of particle sizes to account for polydispersity. Allowance was made for resolution and distribution of wavelengths using a Gaussian function whose width was given by:

$$\sigma^2 = \frac{2\pi}{\lambda}\left[\left(\frac{D_R}{2S_D}\right)^2 + \sin^2\left(\frac{2(R_A+R_B)}{C_D}\right)\right] + \left(\frac{Q\Delta\lambda}{\lambda}\right)^2 \quad (4)$$

where D_R is the detector resolution, S_D is the sample–detector distance, R_A and R_B are respectively the widths of the source and sample diaphragms (where the diaphragm was rectangular, the average of the width and height was used), C_D is the collimation distance, and $\Delta\lambda/\lambda$ is the wavelength distribution (hwhm). The two terms in square brackets are for detector resolution and collimation, while the third term gives the wavelength resolution. This function is similar to the resolution function described by other authors.[16,26,27] A degree of uncertainty arises from the difficulty of precisely defining the source size; for these experiments it was taken as being a 30-mm diameter.

The effects of instrument resolution and polydispersity (which are qualitatively quite similar) are illustrated in Figure 3. It can be seen that, to some extent, the two effects are additive and so both should be included unless one or the other is dominant for the system in question. For a system of polydisperse homogeneous particles the relative scattering intensity is weighted as the sixth power of the radius, while for core–shell latexes, the weighting may vary between 4 and 6 depending on the contrast. This is to account for the difference in volume between a sphere and a hollow shell. Polydispersity for the core–shell latexes may be taken to be in the core or shell radius or both. Best fits to the experimental data were obtained when the polydispersity in the core radius was coupled to that in the shell by:

$$R_c = R_s - \delta \quad (5)$$

where δ is a fixed shell thickness. This is not unreasonable as the polydispersity originates from the seed and the second-stage growth rate is approximately the same for all particles. Some samples were fitted using a "ramp" model (for which an analytic scattering function may also be derived) as illustrated in Figure 1, but it was found that no significant improvement in the fit was obtained. This would suggest that the resolution may be insufficient to discriminate between a true core–shell morphology and a more gradual profile such as that predicted kinetically.

While data were obtained at the extremes of the scattering vector range, the Porod and Guinier regions, these results are not presented here because of difficulties in accurate interpretation.[29] Indeed, there was evidence

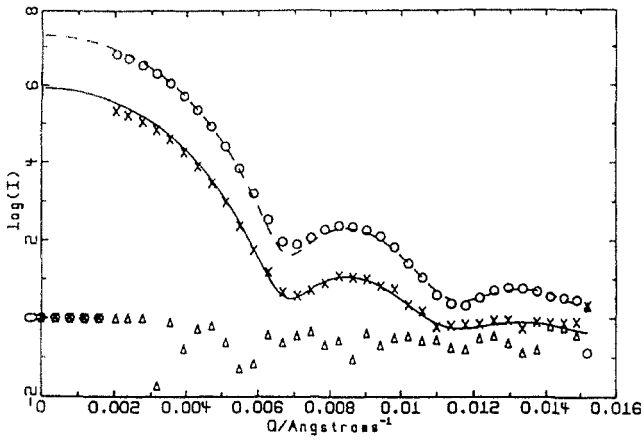

Figure 4. Experimental data and fitted curves for seed latex LS4 (Table III). Experimental data: (○) 20% D_2O, (△) 30% D_2O (contrast-matched), (×) 50% D_2O. Lines: fitted (40% data omitted as these coincided with 20% data).

at low Q of some electrostatic interaction between the particles, which is not unexpected given the relatively high particle concentrations used, together with the intermediate values of the ionic strength probably being insufficient to damp out these interactions. While such data could in principle have been analyzed with an MSA approach, we had no information on the surface potential required to carry out such an analysis. It is felt that our intermediate-Q data have well-defined maxima and minima, and good intensities, and are in a region of Q where charge effects are of negligible importance. Hence, no additional meaningful information could be obtained by Guinier- and Porod-region data analysis.

Results

Seed Latexes (Unswollen). Scattering data were obtained for each sample at four separate contrasts. Results for seed latex LS4 are given in Figure 4, together with fitted curves for each of the contrasts measured. Note that the intensity of the curves scales with the contrast but that the positions of maxima and minima are unaffected. This is the type of behavior expected for scattering from systems of homogeneous spheres.

When the scattering density of the medium is contrast-matched to that of the latex particles (when the aqueous phase is 30% D_2O by weight), there is essentially zero scattering, as the particles are effectively indistinguishable from the medium.

Fitted curves use the homogeneous sphere form of eq 2 with parameters given in Table III. It should be possible to fit the data at all contrasts with a single consistent set of parameters, these being, for a homogeneous particle, as follows: the particle radius, the polydispersity, the scattering densities of the particle and the medium, a scaling factor, and a small amount of residual background. Of these, the scattering densities are known from the latex composition, while reasonable values for the particle radius and polydispersity are known from electron microscopy. The scaling factor may also be calculated if the samples are correctly normalized and the particle number concentration is known. It can be seen that overall the fitted curves are successful in reproducing the experimental data. The small systematic deviations at low Q are probably due to a small amount of interparticle interaction which is typically seen in this Q range; while this effect can be incorporated into the fit, the refinement was not considered warranted in the present case. It is also noted that problems with fitting the depth of the first minimum may be due to small amounts of multiple scattering,[30] consistent with the observation that the discrepancy is most pronounced at high contrast where multiple scattering will be greatest.

The fitting procedure adopted was to use scattering densities calculated from the known composition of the samples (using volume fractions) and then vary the radius, polydispersity, and scaling factor until a satisfactory fit was obtained. Confirmation of the validity of the fits was provided by agreement with the results of electron microscopic measurements, given in Table I. Uncertainties due to fitting were estimated to be *ca.* 10 Å, as determined directly by a standard sensitivity analysis (i.e., alteration of parameters until fit is no longer acceptable). Similarly, the value obtained for the scaling factor was used to calculate the particle number concentration which could then be compared with that predicted from the composition and particle radius. Results showed the predicted values are generally about twice those obtained from fitting. While the following factors may have made some contribution to this error, they do not appear sufficient to explain a difference of this magnitude, and the exact reason for this discrepancy remains uncertain.

(1) The scaling of 20-m data is subject to slight error (due to differing resolutions of the 5- and 20-m data) and may have introduced a systematic error (all 20-m data were scaled by 1/0.0012 to match up with the 5-m data; however, experience has shown that such rescaling works well in practice). However, fitting of corresponding 5- and 20-m data consistently gave the same scaling factor, so such an error seems unlikely.

(2) The presence of surfactant in some samples may also have some effect. Note, however, that, after dilution, the level of surfactant is quite small, and indeed for experiments carried out for seed latex LS4, virtually all surfactant had been removed by dialysis. Furthermore, it is unlikely that the surfactant layer is more than 25 Å in extent (based on the size of the surfactant molecules employed). Results of fitting, e.g., Figure 10, indicate that large effects from surfactant layers are usually not seen: the results shown in this figure are effectively a sensitivity analysis showing the range of models which can fit the data, and hence the possible extent of effects from a surfactant layer, etc. In special cases where there is high contrast due to the surfactant layer, calculations show that significant shifts could occur, but the size and trend of the calculated effects are not consistent with shifts in scattering actually observed due to the presence of internal morphology. This highlights the benefit of measuring scattering at more than one contrast, to eliminate incorrect inferences being drawn from underdetermined data fitting.

(3) It is difficult in practice to know the composition more accurately than this because of uncertainties in solid contents, small sample sizes, and possible losses by evaporation. Also such errors would probably not be systematic. It is noted that careful NMR measurements might be able to give more accurate compositions.

While the source of the error in normalization could not be found, results are at the very least internally consistent. The normalization is not critical to the analysis of the morphology as it does not directly affect the particle form factor (which contains most of the information about the morphology) but merely scales all of the data sets by the same amount. If the data are consistent, it is therefore fair to say that all parameters used in the fit are known prior to the experiment and this necessarily constrains the fitting procedure (e.g., the radius obtained from electron microscopy should not be significantly different

Table III. Fitted Parameters[a]

latex	% D_2O	R (nm)	σ (nm)	ρ_p[b]	ρ_m[b]	SF ($\times 10^{-14}$)	ratio N_c calc/fit	bgrd
LS4	20	67	3.0	1.42	0.729	1.1	2.1	1.0
	30			contrast matched				
	40	67	3.0	1.42	2.07	1.2	2.1	0.85
	50	67	3.0	1.42	2.80	1.4	2.1	0.90
DEU10	0	58	3.0	6.47	−0.56	5.0	2.1	1.0
S40NM	20[c]	45	4.0	1.42	0.729	1.0	2.0	1.0
	30			contrast matched				
	40	45	4.0	1.42	2.07	3.5	2.7	1.0
	65	45	4.0	1.42	3.82	3.5	2.3	1.0
				Swollen Latexes				
LS4	20	82	3.0	3.525	0.729	0.85	1.8	1.5
	30	82	3.0	3.525	1.39	1.0	1.8	1.0
	40	82	3.0	3.525	2.07	1.0	1.8	1.0
	50	82	3.0	3.525	2.75	1.0	2.0	1.2
DEU10	99	77	3.0	3.70	6.40	2.0	2.5	0.5

[a] SF is the scaling factor used in the fit; p and m denote particle and medium, respectively. [b] Units are 10^{-10} cm^{-2}. [c] Solids content 2.35%.

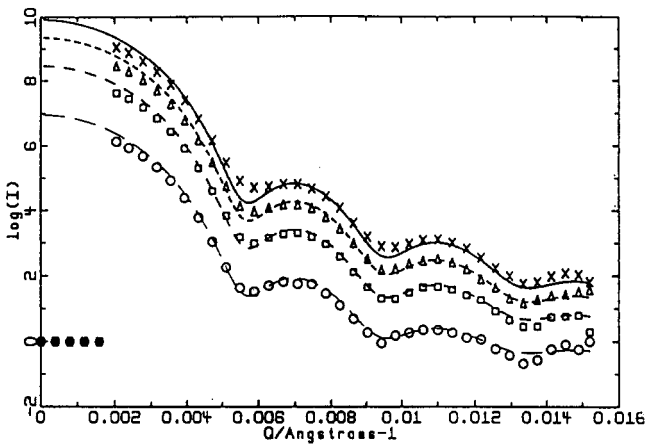

Figure 5. Experimental data and fitted curves for swollen latex LS4 (Table III). Experimental data: (×) 20% D_2O; (△) 30% D_2O; (□) 40% D_2O; (○) 50% D_2O. Lines: fitted.

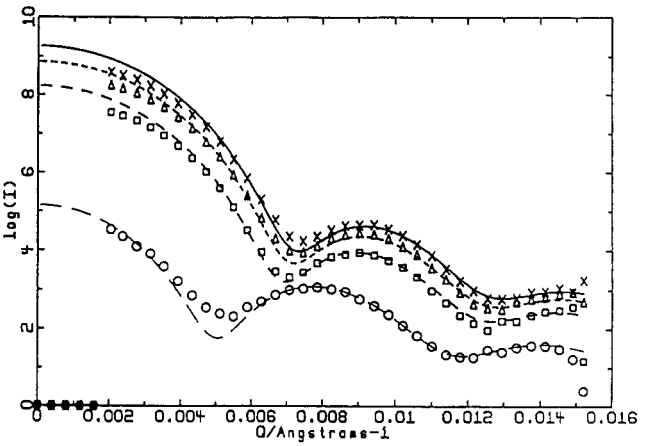

Figure 6. Experimental data and fitted curves for two-stage latex DEU7 (Table IV). Experimental data: (×) 20% D_2O; (△) 30% D_2O; (□) 40% D_2O; (○) 50% D_2O. Lines: fitted.

from the overall radius from SANS). What is important is that the method is demonstrated to be capable of detecting inhomogeneities in these systems.

Swollen Latexes. Having carried out basic checks on the scattering data for seed latexes, we now examine the scattering from the swollen latexes for evidence of inhomogeneity. On inspection of the results for the swollen latexes, it is again found (Figure 5) that the scattering curves scale with contrast. A consistent fit is obtained to the homogeneous sphere model for all contrasts (as was the case for the seed latexes) with an increased particle radius in quantitative agreement with that expected from swelling (Table III). The value of ρ_p was adjusted slightly to obtain a consistent value of the scaling factor for all contrasts: about 10% lower than might be expected purely on the basis of the weight ratio of polystyrene to toluene. This is due in part to the presence of toluene in the aqueous phase. The solubility of toluene in water is about 5×10^{-3} mol dm^{-3},[31] slightly higher than that of styrene. For a sample having 1% solids, this amounts to about 5% of the total toluene in the system. Some toluene may also be lost because of evaporation, the vapor pressure of toluene in air being *ca.* 30 Torr at 30 °C. This amounts to a toluene headspace concentration of at least 2×10^{-3} mol dm^{-3}, and so assuming that the volume of air in the container used for swelling was approximately equal to that of the sample (the possible significance of this factor was not realized at the time of measurement), there may be significant loss of material by evaporation.

The scattering from one of the samples was again measured after a further 48 h had elapsed, with no appreciable change being observed. This indicates that the swollen latexes were quite stable. The fits obtained for these samples would not be possible if there were significant inhomogeneities in the swollen particles (see results for the two-stage latexes). It is concluded therefore that swelling is essentially uniform and that repulsive wall effects are not a significant cause of inhomogeneity. This conclusion is consistent with results of other workers.[16]

Seeded Polymerizations. Next, we examine systems where a core–shell morphology has been deliberately promoted by a step-growth seeded polymerization. Scattering and fitted curves for the two-stage latex DEU7 are shown as a function of contrast in Figure 6 (parameters in Table IV). It can be seen that, as the scattering density of the medium approaches that of the particle, there is a sudden shift in the positions of the minima. This behavior is quite different to that observed for the seed and swollen latexes but is consistent with the scattering behavior predicted by the core–shell model (Figure 2). When the contrast between the particle and medium is far greater than that between the core and shell, the density profile resembles, to a good approximation, that of a homogeneous sphere. If, on the other hand, the scattering density of the medium is close to that of the core or the shell, considerable shifts in the scattering are expected.

Attempts to fit the scattering to a homogeneous sphere model (Figure 7 and Table V) were unsuccessful even at high contrast (low % D_2O) where this model might be expected to be a more reasonable approximation. As seen in Figure 7, the experimental data show elevated intensity

Table IV. Fitted Parameters: Two-Stage Latexes[a]

latex	% D_2O	R_s[b]	R_c	σ (nm)	ρ_c[b]	ρ_s	ρ_m	SF	bgrd
DEU11	20	81	74	4.0	3.28	5.0	0.73	8.0×10^{-14}	0.5
DEU11	30	81	74	4.0	3.28	5.0	1.39	8.0×10^{-14}	0.5
DEU11	40	81	74	4.0	3.28	5.0	2.07	8.0×10^{-14}	0.5
DEU11	60	81	74	4.0	3.28	5.0	3.46	8.0×10^{-14}	0.5
DEU7	20	56	42	4.5	3.05	4.5	0.73	2.7×10^{-14}	0.5
DEU7	30	56	42	4.5	3.05	4.5	1.39	2.7×10^{-14}	0.5
DEU7	40	56	42	4.5	3.05	4.5	2.06	2.7×10^{-14}	0.5
DEU7	60	56	42	4.5	3.04	4.5	3.46	2.7×10^{-14}	0.5
DEU3	20	55	45	4.0	3.6	4.3	0.73	2.6×10^{-14}	0.5
DEU3	30	55	45	4.0	3.6	4.3	1.39	2.6×10^{-14}	0.5
DEU3	40	55	45	4.0	3.6	4.3	2.07	2.6×10^{-14}	1.2
DEU3	90	54	52	4.0	4.0	0.35	5.71	2.6×10^{-14}	1.5

[a] c, s, and m denote core, shell, and medium, respectively. [b] Radii are in nanometers; scattering length densities are $\rho \times 10^{10}$ cm^{-2}.

Table V. Fitted Parameters: Various Models

fit	% D_2O	R_s	R_c	σ (nm)	ρ_c	ρ_s	ρ_m	scaling	bgrd
				Figure 7: DEU7 20% D_2O					
a	20	56	42	4.5	4.0	4.0	0.73	2.5×10^{-14}	0.5
b	20	56	54	4.5	4.0	0.35	0.73	2.5×10^{-14}	0.5
c	20	56	42	4.5	3.05	4.5	0.73	2.5×10^{-14}	0.5
				Figure 10: DEU3 20% D_2O					
d	20	55	45	4.0	4.0	4.0	0.729	2.6×10^{-14}	1.5
e	20	55	53	4.0	4.0	0.35	0.729	2.6×10^{-14}	1.5
f	20	55	45	4.0	3.6	4.3	0.729	2.6×10^{-14}	1.5
g	20	55	45	4.0	3.2	5.0	0.729	2.6×10^{-14}	1.5
				Figure 11: DEU3 90% D_2O					
h	90	55	45	4.0	3.6	4.3	5.64	2.7×10^{-14}	1.5
i	90	55	52	4.0	4.0	4.0	5.64	2.7×10^{-14}	1.5
j	90	55	54	4.0	4.0	0.35	5.64	2.7×10^{-14}	1.5

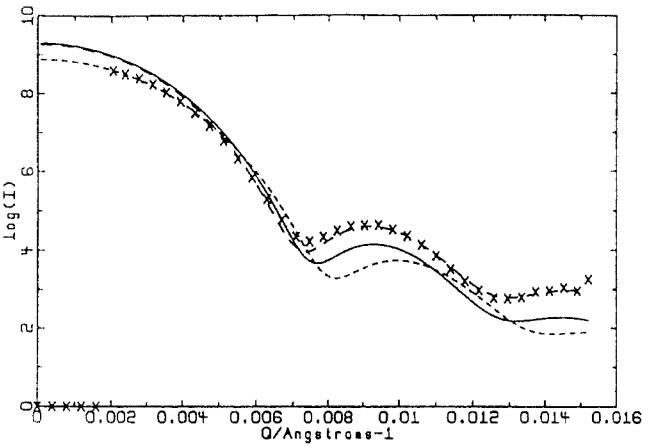

Figure 7. Comparison of core–shell and homogeneous fits for two-stage latex DEU7 (20% D_2O). See Table V. (—) Homogeneous model (a). (···) Homogeneous model with surfactant layer (b). (- - -) Core–shell model (c). (×) Experiment.

at high scattering angles, this being indicative that some additional "structure" is producing an enhancement in the scattering function. Fitting to a core–shell model showed greatly improved results, with a reasonably consistent parameter set over all contrasts. While there is some room for improvement in the fits, it is recognized that the core–shell model is only an approximation and that the true form of the density profile is not known. Given this, results are surprisingly good.

There are two additional parameters in the core–shell model: (1) the radius of the core (not necessarily equal to the seed radius) and (2) the scattering length densities of the core and shell in place of the average particle scattering length density.

These parameters are subject to the constraint that the scattering length density averaged over the entire particle is known. All parameters including ρ_c and ρ_s were varied

Table VI. Comparison of Predicted and Fitted Parameters: Two-Stage Latexes

latex	% D_2O	ρ_{av}(fitted)	ρ_{av}(calc)	N_c calc/fit
DEU11	20	3.69	3.85	2.06
DEU11	30	3.69	3.85	2.14
DEU11	40	3.69	3.85	2.10
DEU11	60	3.69	3.85	2.14
DEU7	20	3.89	3.85	1.98
DEU7	30	3.89	3.85	1.98
DEU7	40	3.89	3.85	1.98
DEU7	60	3.89	3.85	1.98
DEU3	20	3.77	3.85	2.34
DEU3	30	3.77	3.85	2.34
DEU3	40	3.77	3.85	2.34
DEU3	90	3.77	3.85	2.34

until the best possible fit was obtained. From the values of the fitted parameters, it is found for both DEU7 and DEU11 that the core radius corresponds roughly with that of the seed, with the shell containing approximately 60–70% deuterated polystyrene and the core 30–40%. Good agreement of the particle radius with EM results is again obtained (cf. Table I). The average densities are also found to be close to the expected values (Table VI). The slightly lower fitted values may have been due to some monomer loss during polymerization (note a slight excess of styrene-d_8 (3–4%) was initially added in the case of DEU7). Results suggest significant intermixing of core and shell polymers as predicted by the kinetic simulations of morphology arising at high conversions.[1] The extent of morphology is also seen to be similar, although the precise shape of the profile is beyond the resolution of this experiment. This is borne out by results obtained using the analytic form for a ramp function (Figure 8) which appear to fit the data equally well (note that the number of parameters is the same as in the core–shell model).

While fits to sample DEU11 gave very similar results to DEU7 (Figure 9 and Table V), sample DEU3 showed

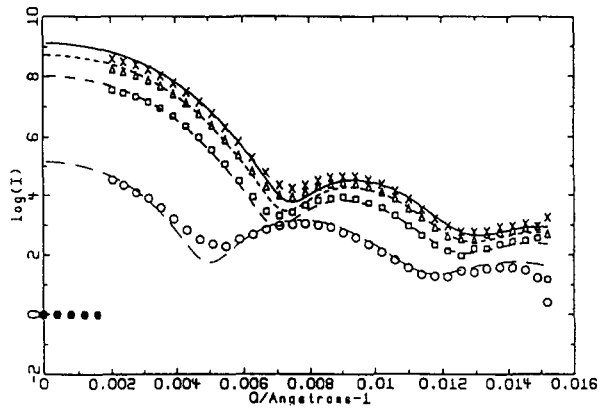

Figure 8. Fit of latex DEU7 to ramp model (Table V). Experimental data: (×) 20% D_2O; (△) 30% D_2O; (□) 40% D_2O; (○) 60% D_2O. Lines: fitted.

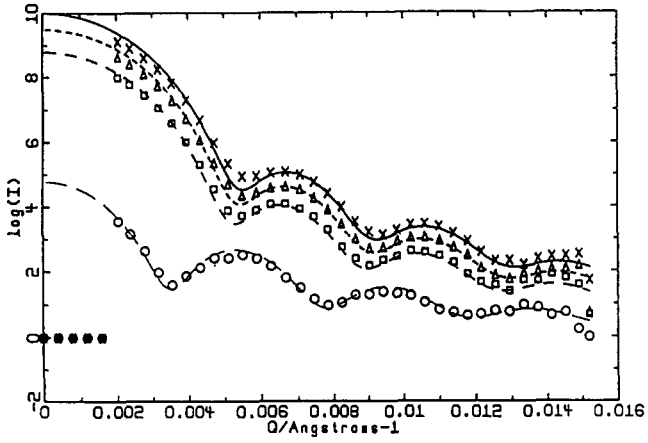

Figure 9. Experimental data and fitted curves for two-stage latex DEU11 (Table IV). Experimental data: (×) 20% D_2O; (△) 30% D_2O; (□) 40% D_2O; (○) 60% D_2O. Lines: fitted.

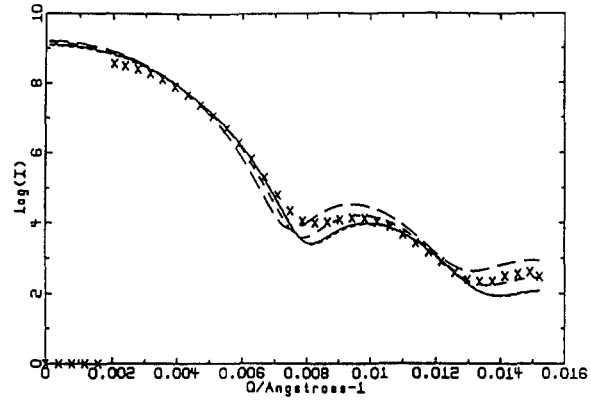

Figure 10. Comparison of fits for two-stage latex DEU3 (20% D_2O, Table V). (—) Homogeneous model (d). (···) Homogeneous model with surfactant layer (e). (- - -) Core–shell model (f). (– –) Core–shell model, high contrast between core and shell (g). (×) Experiment.

quite different behavior. The different contrasts used for this sample must however be taken into consideration here as will be seen below. Fits for low % D_2O data seem consistent with a reduced level of inhomogeneity (Figure 10). Some indication of the *sensitivity* of the fits to the extent of inhomogeneity here is given by Figures 7 and 10.

Results of fitting the 90% D_2O sample to both the homogeneous and core–shell models were relatively poor and a degree of improvement could only be obtained if a shell of low scattering length density was included (Figure 11 and Table V; note further improvement might be achieved by using a multishell model for this sample, one

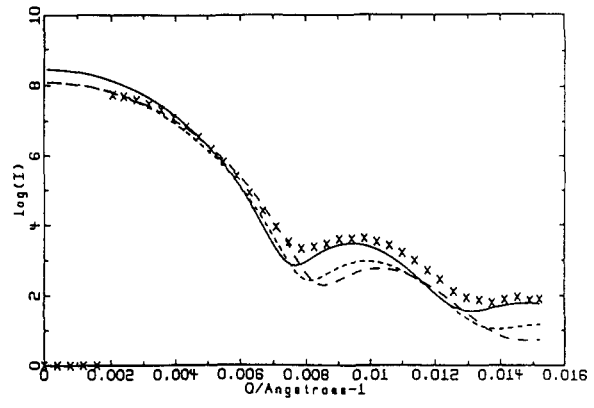

Figure 11. Comparison of fits for two-stage latex DEU3 (90% D_2O, Table V). (···) Core–shell model (h). (—) Surfactant layer (j). (- - -) Homogeneous model (i). (×) Experiment.

shell representing surfactant). This suggests the surfactant layer may be contributing to the scattering, and for these polymerization recipes, surfactant coverage for this sample is around 100%. While it would in retrospect have been preferable to remove surfactant, its presence is not necessarily a problem for low D_2O/H_2O ratios because the scattering is found to be relatively insensitive to the presence or absence of a surfactant layer at these contrasts (see Figures 7 and 10). (Likewise the scattering at 90% D_2O is insensitive to the internal morphology). Because of the difficulties described with sample DEU3, the precise extent of inhomogeneity in this sample is not clear. Nonetheless, the sensitivity appears sufficient to conclude that the level of inhomogeneity (if any) is reduced in this sample. In retrospect, more scattering data in the range 40–80% D_2O would have been desirable for all samples as (in the absence of surfactant) this would be the region most sensitive to the morphology. The optimal range will of course vary from sample to sample.

Consideration of the data for the two-stage latexes shows that significant inhomogeneity is observed in at least two of the three samples. This may be understood in the context of the surface anchoring model as follows: If one uses the radius of gyration of the second-stage polymer as an indication of its effective penetration range, it can be seen that those latexes which show most evidence of inhomogeneity are in fact those in which one would expect to see the greatest effect. Assuming an effective penetration depth for anchored chains of approximately 1–2 times the polymer radius of gyration R_g, it can be seen that, in the case of latex DEU3, second-stage polymer should penetrate considerably further than in DEU7 and DEU11. It is interesting to note that the samples which exhibit core–shell type morphology also fall in the range of R_g/R_f (where R_f is the particle radius) predicted by Yang *et al.*[3] to show significant repulsive wall effects. However, in light of the swelling experiments of the current work, it is concluded that the morphology is not a result of repulsive wall effects. It seems somewhat coincidental that similar criteria for inhomogeneity appear to apply to both models.

One final point which should be kept in mind when using isotopically labeled polymers is that incompatibility of protonated and deuterated species may in some circumstances give rise to phase separation. Since the entropy of mixing is relatively small for polymer blends, very small positive enthalpy terms may become important in these systems. While such effects have been observed,[32] they are most pronounced for polymers of very high molecular weight and are not believed to be important in the present work. Consistent with this is the observation

that DEU3 has the highest molecular weight of our samples but exhibits the least morphology.

Conclusions

Scattering from swollen latexes was found to be consistent with uniform swelling, contrary to what has sometimes been suggested in the literature from considerations of repulsive wall effects. That is, any contribution to a core–shell morphology arising solely from the entropic drive of chains toward the center of a particle is negligible. This result is consistent with the theoretical calculations[2] and with results from fluorescence and other scattering studies.[30,33] The conventional picture of uniform *monomer* distribution in most emulsion homopolymerizations appears to be correct.

Results from two-stage polymerizations, however, show that surface anchoring effects may give rise to nonuniform polymerization. Results appear consistent with predictions of kinetic simulations.[1] While data obtained thus far are promising, more extensive studies are required for it to be possible to predict the morphology with complete confidence over a range of experimental conditions. What is most encouraging is that the relatively simple contrast variation techniques described give (with careful choice of contrast points) useful insight into the morphology of these systems and may provide useful guidelines for future investigations of surface anchoring, repulsive wall, and other morphological phenomena.

Acknowledgment. The support of the Australian Research Grants Scheme, the Institut Laue–Langevin, and the Science and Engineering Research Council and of an Australian Postgraduate Research Award for M.F.M. is gratefully acknowledged, as is the Sydney University Electron Microscope Unit for generous provision of facilities.

References and Notes

(1) Mills, M. F.; Gilbert, R. G.; Napper, D. H. *Macromolecules* **1990**, *23*, 4247.
(2) Mills, M. F.; Gilbert, R. G.; Napper, D. H.; Croxton, C. A. *Macromolecules*, following paper in this issue.
(3) Yang, S. I.; Klein, A.; Sperling, L. H.; Casassa, E. F. *Macromolecules* **1990**, *23*, 4582.
(4) Yang, S. I.; Klein, A.; Sperling, L. H. *J. Polym. Sci., Polym. Phys. Ed.* **1989**, *27*, 1649.
(5) Chen, S. A.; Lee, S. T. *Makromol. Chem. Rapid Commun.* **1990**, *11*, 443.
(6) Grancio, M. R.; Williams, D. J. *J. Polym. Sci., Polym. Chem. Ed.* **1970**, *8*, 2617.
(7) Keusch, P.; Williams, D. J. *J. Polym. Sci., Polym. Chem. Ed.* **1973**, *11*, 143.
(8) Nomura, M.; Ikoma, J.; Fujita, K. In *Polymer Latexes—Preparation, Characterization and Applications*; Daniels, E. S., *Sudol*, E. D., El-Aasser, M., Eds.; ACS Symposium Series 492; American Chemical Society: Washington, DC, 1992; p 55.
(9) Alduncin, J. A.; Forcada, J.; Barandiaran, M. J.; Asua, J. M. *J. Polym. Sci. Part A: Polym. Chem.* **1991**, *29*, 1265.
(10) Keusch, P.; Graff, R. A.; Williams, D. J. *Macromolecules* **1978**, *7*, 304.
(11) Chang, H. S.; Chen. S.-A. *Makromol. Chem., Rapid Commun.* **1987**, *8*, 297.
(12) van den Hul, H. J.; Vanderhoff, J. W. *Br. Polym. J.* **1970**, *2*, 121.
(13) Linne, M. A.; Klein, A.; Sperling, L. H.; Wignall, G. D. *J. Macromol. Sci., Phys.* **1988**, *B27*, 181.
(14) Dabdub, D.; Klein, A.; Sperling, L. H. *J. Polym. Sci., Part B: Polym. Phys.* **1992**, *30*, 787.
(15) Fisher, L. W.; Melpolder, S. M.; O'Reilly, J. M.; Ramakrishnan, V.; Wignall, G. D. *J. Colloid Interface Sci.* **1988**, *123*, 24.
(16) Harris, N. M.; Tabony, J.; Goodwin, J.; Ottewill, R. H. *J. Colloid Interface Sci.* **1980**, *78*, 253.
(17) Bootle, G. A.; Lye, J. E.; Ottewill, R. H. *Makromol. Chem., Macromol. Symp.* **1990**, *35*, 291.
(18) Whang, B. C. Y.; Ballard, M. J.; Napper, D. H.; Gilbert, R. G. *Aust. J. Chem.* **1991**, *44*, 1133.
(19) Hawkett, B. S.; Napper, D. H.; Gilbert, R. G. *J. Chem. Soc., Faraday Trans. 1* **1980**, *76*, 1323.
(20) Mills, M. F. Ph.D. Thesis, University of Sydney, Sydney, Australia, 1992.
(21) Clay, P. A.; Gilbert, R. G.; Napper, D. H. Manuscript in Preparation.
(22) *Polymer Handbook*, 3rd ed.; Brandrup, A.; Immergut, E. H., Eds.; Wiley-Interscience: New York, 1989.
(23) Guinier, A.; Fournet, G. *Small angle scattering of X-rays*; Wiley: New York, 1955.
(24) Markovic, I.; Ottewill, R. H.; Cebula, D. J.; Field, I.; Marsh, J. F. *Colloid Polym. Sci.* **1984**, *262*, 648.
(25) Ghosh, R. E. A computing guide for small-angle scattering experiments. Report No. 89 GH02T; Institut Laue-Langevin: Grenoble, France, 1989.
(26) Pederson, J. S.; Posselt, D.; Mortensen, K. *J. Appl. Crystallogr.* **1990**, *23*, 321.
(27) Mildner, D. F. R.; Carpenter, J. M. *J. Appl. Crystallogr.* **1984**, *17*, 249.
(28) Ghosh, R. E. FITFUN: An interactive/graphical fitting routine. Report No. 89GHO8T; Institut Laue-Langevin: Grenoble, France, 1989.
(29) Ciccariello, S.; Goodisman, J.; Brumberger, H. *J. Appl. Crystallogr.* **1987**, *21*, 117.
(30) Harris, N. M. D. Phil. Thesis, Oxford University, Oxford, U.K., 1980.
(31) Stephen, H.; Stephen, T. *Solubilities of inorganic and organic compounds*; Pergamon Press: London, 1979.
(32) Wignall, G. D.; Bates, F. S. *Makromol. Chem., Macromol. Symp.* **1988**, *15*, 10.
(33) Huelin, X.; Winnik, M. A.; Satguru, R. *Makromol. Chem., Macromol. Symp.*, in press.